Engineering Analysis with Boundary Elements 144 (2022) 67–80

Contents lists available at ScienceDirect

Engineering Analysis with Boundary Elements

journal homepage: www.elsevier.com/locate/enganabound

Boundary element model for the analysis of the dynamic response of the Soria arch dam and experimental validation from ambient vibration tests

J.C. Galván, L.A. Padrón *, J.J. Aznárez, O. Maeso

Instituto Universitario de Sistemas Inteligentes y Aplicaciones Numéricas en Ingeniería (SIANI), Universidad de Las Palmas de Gran Canaria (ULPGC), Edificio Central del Parque Científico y Tecnológico, Campus Universitario de Tafira, Las Palmas de Gran Canaria, 35017, Spain

ARTICLE INFO

Keywords:
Arch dams
Boundary element method
Soil–structure interaction
Fluid–structure interaction
Dynamic analysis
Modal identification

ABSTRACT

This paper presents a 3D boundary element time–harmonic model for the analysis of the dynamic behavior, under low-level vibrations, of the Soria arch dam (Gran Canaria, Spain). The model takes into account dynamic Soil–Structure Interaction (DSSI), Fluid–Structure Interaction (FSI) and the actual geometry of dam wall and reservoir. The rock and the dam wall are considered as viscoelastic regions, and the water in the reservoir is modeled as an inviscid fluid. The influence of DSSI, FSI, height of the water in the reservoir, accuracy of the geometric modeling of the canyon, and type of transmitting boundary conditions at the truncated end of the reservoir, are evaluated. DSSI and FSI have a significant influence on the dynamic response of the dam, and the accurate representation of the geometry of the canyon is relevant for the correct estimation of the modal shapes. Ambient vibrations tests were also performed, from which the first and third modes could be clearly identified. The comparison between the experimental and numerical natural frequencies and mode shapes suggests that the proposed complete numerical model is able to capture the dynamic response and can be used for the structural health monitoring of the wall of this dam.

1. Introduction

The Soria arch dam is a double curvature concrete arch dam located in Gran Canaria (Spain) with a height above the foundation of 120 m, a gross capacity of the reservoir of 32 Hm^3, a quasi-symmetrical geometry and a total crest length of approximately 150 m. Built between 1962 and 1972, it is now planned to be part of the Chira–Soria pumped-storage hydroelectric power station project, that plans to take advantage of the already existing reservoirs of Chira and Soria to create a system with an energy storage capacity of 3.2 GWh, with the aim of increasing the integration of renewable energies in the island by 2026 and improving the stability of its isolated electricity system.

Structural Health Monitoring (SHM) of dams is already common practice as support for managing, maintenance and assessment of the level of security of these critical infrastructures [1]. Numerical models are key parts of these SHM systems. The Boundary Element Method (BEM) and the Finite Element Method (FEM) have both been used to study the dynamic response of arch dams through modal, frequency-domain and time-domain numerical analyses. These methodologies also allow to take into account the flexibility of the foundation, and study the relevance of the dam–reservoir–foundation interaction in the response of the system. For instance, the steady-state harmonic response of the Morrow Point arch dam was studied using the FEM by Fok and Chopra [2,3] for a wide range of parameters characterizing the properties of the dam, the full or empty reservoir, the mathematical representation of the truncated reservoir boundary (rigid or absorptive) and the consideration of the foundation rock as rigid or flexible. Later, Tan and Chopra [4] improved the model, included the inertia and damping of the foundation rock, and performed a wider parametric analysis. The same case of study was addressed by Domínguez and Maeso [5,6] using a multi-region three-dimensional coupled BEM technique for the steady-state harmonic analysis of the linear seismic response of arch dams including the compliant foundation, the presence of water and reservoir geometry, and complex phenomena such as the traveling-waves effects. Later, Maeso et al. [7] continued the development of the model and studied the effects of the ground motion spatial variation and of the canyon geometry on the response of the Morrow Point arch dam under seismic waves impinging the site from different directions and considering several canyon and reservoir geometries. Afterwards, Maeso et al. [8] and Aznárez et al. [9] enhanced the model to include the presence of bottom sediments using the Biot's poroelastic formulation, and analyzed the influence of sediments on the dynamic and seismic response of the system,

* Corresponding author.
E-mail addresses: juancarlos.galvan@ulpgc.es (J.C. Galván), luis.padron@ulpgc.es (L.A. Padrón), juanjose.aznarez@ulpgc.es (J.J. Aznárez), orlando.maeso@ulpgc.es (O. Maeso).

https://doi.org/10.1016/j.enganabound.2022.08.008
Received 11 July 2022; Received in revised form 2 August 2022; Accepted 4 August 2022
Available online 19 August 2022

and García et al. [10,11] used the model to study how the reservoir level, the thickness of the sediments, or the angles of incidence of the seismic waves affect the computed seismic response of the dam. Other computational schemes have also been proposed. For instance, Seghir et al. [12] presented a FEM–symmetric BEM 2D model for the study of the dam–reservoir interaction problem in gravity dams considering the reservoir domain as unbounded. Later, Aftabi and Lotfi [13] presented a Finite Element-(Finite Element-Hyper Element)-Boundary Element method for the dynamic analysis of arch dams, including a modal approach and fluid finite elements to discretize the near-field region of the reservoir, and three-dimensional fluid hyperelement to model the prismatic channel that extends to infinity. Recently, Li et al. [14] proposed a new 3D scaled boundary finite element method (SFBEM) to study the dam–rock foundation interaction of arch dams taking into account the inclined layered half-space. The Soria arch dam, in particular, was recently studied, from the static point of view, by Concepción–Guodemar et al. [15], who developed a detailed three-dimensional finite-differences model to study the distribution of stresses in the dam under static conditions. For a deeper literature review on the models employed to study the dynamic response of concrete arch dams, the reader is referred to Rezaiee–Pajand et al. [16].

The influence of the reservoir topology, and the study of the mathematical representation of the truncated boundary of the reservoir, are other aspects that are relevant to this problem and to the numerical models that are used. Specific boundary conditions to represent the truncated boundary of the reservoir have been developed and applied to this problem by numerous authors, such as Humar and Roufaiel [17], Medina and Domínguez [18,19], Fok and Chopra [2,3], Domínguez and Meise [20], Szczesiak and Weber [21], Maeso et al. [7,8], Aznárez et al. [9], Aftabi and Lotfi [13], or Jafari and Lotfi [22]. The influence of how the geometry of the reservoir is modeled is another aspect of interest. For instance, García et al. [10] studied the influence of considering an open or a closed reservoir. Mircevska et al. [23] focused on the influence of the distance of the truncated boundary from the dam wall, and Mircevska et al. [24] looked into how the geometry of the reservoir (with a regular or a complex surface) affects the distribution of the hydrodynamic forces over the dam wall due to the seismic actions.

The modal analysis of these arch dams is another approach that contributes to a deeper understanding of the dynamics of the system. Two dedicated studies on this matter are, for instance, those of Farzad and Lotfi [25], and Hariri-Ardebili et al. [26]. From the experimental point of view, ambient vibration techniques allow to study different aspects of the dynamic behavior of dams, and make possible to identify natural frequencies and mode shapes. In fact, ambient vibration techniques have been applied with success to the experimental study of several arch dams in the last two decades. For instance, the arch dams of Mauvoisin, Ounta Gennarta, La Tajera, Baixo Sabor or Saint–Guérin were identified and studied by Darbre et al. [27,28], Calcina et al. [29], García-Palacios et al. [30], Pereira et al. [31] and Guo et al. [32], respectively. The state of the art of this issue has been recently summarized by Pereira et al. [33].

As said above, numerical models can be used in SHM applications to inform in the design of the monitoring system and to analyze the measured data but, at the same time, such models are always subject to a certain level of uncertainty due to the assumptions and simplifications made during its development regarding, for instance, material properties, geometries, boundary conditions and governing laws of the different regions involved. In this line, the objective of this study is threefold: on the one hand, it aims at building a three-dimensional boundary element numerical model of the Soria arch dam for the analysis of its dynamic response under low-level vibrations; on the other hand, it aims at evaluating the influence of three different aspects that can be subject to different levels of simplification during the process of development of the model. These three aspects are: (a) the relative flexibility of the foundation rock, which is related to how relevant are the dynamic soil–structure interaction effects on the response of the dam wall; (b) the accuracy of the geometrical representation of the surrounding topography, which is related to whether the computed results are influenced by a geometrical simplification of the canyon of the reservoir; and (c) the way in which a truncated reservoir is considered in the model, which is related to the influence of the type of boundary condition used to represent the continuation of the body of water, and the propagation of waves away from the wall. The final objective, after having studied the items listed above, is to validate and update the numerical model by comparing the main modal parameters against those determined by ambient vibrations tests.

2. Problem definition

2.1. The soria arch dam

The Soria dam is located in the south of the Island of Gran Canaria (one of the Canary Islands, Spain). It is the highest dam in the archipelago (120 m high) and forms the largest reservoir, with a capacity of 32 Hm^3, although it has never exceeded 40% of its capacity. The dam wall, built between 1962 and 1972 [34], is a concrete double-curvature arch dam (see Fig. 1) with a variable radius, quasi-symmetrical geometry and a total crest length of approximately 150 m. The spillway is situated on the left side (looking from upstream). The thickness of the wall decreases from 17.30 m at the base to 3 m at the crest.

2.2. Geometrical models for the analysis of the dam

The geometry of the dam wall was generated from the topological information provided in a specific study of the dam developed nearly twenty years after its completion [35]. On the other hand, the geometrical representation of the actual topography and surroundings was constructed from lidar topographic information [36]. In order to study not only the dynamic properties of the dam wall, but also the influence of DSSI, water level and accuracy of the geometrical representation of the canyon, four different geometrical models of the system have been built: a model including only the dam wall for studies assuming a fixed-base boundary condition at the abutments and foundation (see Fig. 1b) and three compliant-base models (see Fig. 2) that include a model with a simplified straight trapezoidal canyon and an amount of free-surface around the dam wall equivalent to twice the height H of the dam wall (Fig. 2a), a model with a more realistic topographical representation of the canyon (built from lidar data) and also with an amount of free-surface around the dam wall equivalent to twice the height H of the dam wall (Fig. 2b), and another simplified model with a straight trapezoidal canyon but an amount of free-surface around the dam wall equivalent to three times the height H of the dam wall (Fig. 2c) used to check the influence of this parameter on the numerical results. The BE meshes consist of nine-node quadratic quadrilateral elements and six-node quadratic triangular elements. The boundary element mesh of the dam wall was validated by comparison of the natural frequencies and mode shapes of the fixed-base dam wall against those obtained from a modal analysis of a finite element model. Table 1 summarizes the number of nodes and elements of the validated meshes finally used in this analyses presented below.

Both the dam wall and the rock in the foundation and the reservoir are assumed as viscoelastic solid materials, while the response of water media is modeled as acoustic media, described by the Helmholtz's

Table 1
Number of BEM nodes and elements in the different models.

BEM models	Number of nodes	Number of elements
Fixed base (dam wall only)	3228	733
Compliant base, trapezoidal canyon ($R = 2H$)	8168	2023
Compliant base, topographic canyon ($R = 2H$)	10 397	2739
Compliant base, trapezoidal canyon ($R = 3H$)	10 408	2631

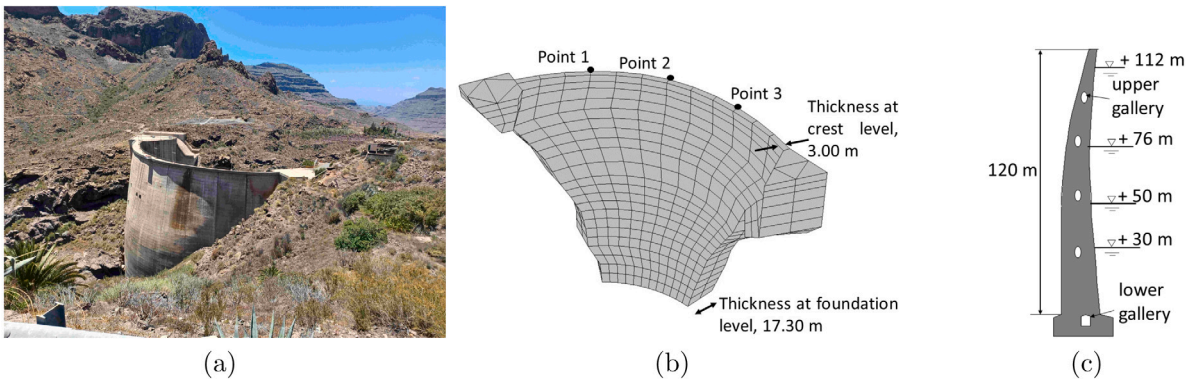

Fig. 1. Soria dam. (a) Soria reservoir general view (b) Dam wall representation (c) Dam wall cross section. Points 1, 2 and 3 are located approximately at 1/4, 1/2 and 3/4 of the dam crest, respectively, measured from left to right abutment.

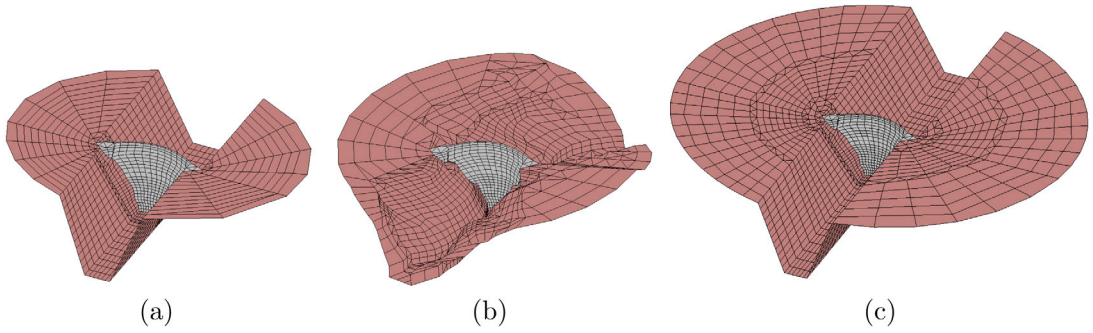

Fig. 2. Geometrical models and meshes of the reservoir. (a) straight trapezoidal canyon with $R = 2H$, (b) topographic canyon with $R = 2H$, and (c) straight trapezoidal canyon with $R = 3H$.

Table 2
Initial mechanical properties assumed for the concrete in the dam wall and for the surrounding rock.

Material property	Concrete	Rock	Water
Shear modulus, G (GPa)	8.16	12.1	–
Density, ρ (kg/m^3)	2300	2143	1000
Poisson's ratio, ν	0.2	0.2	–
Damping ratio, ξ	0.01	0.01	–
Pressure wave velocity (m/s)			1438

equation. Table 2 presents the material properties initially considered for each one of the regions. The mechanical properties of the concrete in the dam wall are initially extracted from the specific study on the Soria dam [35]. The mechanical properties of the rock, on the other hand, correspond to generic properties of the ignimbrite rocks found in the location. Frequency-independent hysteretic material damping in the solid regions is considered through the definition of complex elastic properties of the type $G = \mathrm{Re}[G](1+2\mathrm{i}\xi)$, being ξ the hysteretic damping ratio. Five different possibilities were considered with respect to the water level in the reservoir: empty reservoir and water levels of 30, 50, 76 and 112 m (see Fig. 1c).

3. Governing equations

This section describes in detail the main aspects of the mathematical models used in this study. It presents the models employed to represent the steady–state dynamic behavior of the different regions of the problem, the types of boundary conditions defined to represent the truncated boundaries of the reservoir, the representation of the input seismic excitation and also the way in which all these different equations are coupled to solve the problem.

3.1. Dam wall and foundation rock

The dam wall and the foundation rock are modeled as viscoelastic isotropic regions whose behavior can be represented by the Navier's equations that, in the frequency domain, can be written as

$$G\left[\nabla^2\mathbf{u} + \frac{1}{1-2\nu}\nabla(\nabla\mathbf{u})\right] + \rho\omega^2\mathbf{u} = \mathbf{0} \tag{1}$$

where $\mathbf{u}(x, y, z, \omega)$ is the field of displacements, G, ν and ρ are the shear modulus, Poisson's ratio and density of each medium, and ω is the circular frequency. The dynamic response of such region can be represented through the Boundary Integral Equation (BIE) for the displacements $\mathbf{u}(x, y, z, \omega)$ and tractions $\mathbf{t}(x, y, z, \omega)$, along the boundaries Γ, written for a collocation point $\mathbf{x}^k$:

$$\mathbf{c}^k\mathbf{u}^k + \int_\Gamma \mathbf{t}^*\mathbf{u}\,\mathrm{d}\Gamma - \int_\Gamma \mathbf{u}^*\mathbf{t}\,\mathrm{d}\Gamma = \mathbf{0} \tag{2}$$

where $\mathbf{u}^*$ and $\mathbf{t}^*$ are the elastodynamic fundamental solution tensors for a time harmonic Dirac Delta function at point $\mathbf{x}^k$, and $\mathbf{c}^k$ is the local free term matrix at the same point. After the discretization of the domains using appropriate boundary elements, Eq. (2) can be applied on every node for the three directions of space, which allows building a system of equations of the type

$$\mathbf{Hu} - \mathbf{Gt} = \mathbf{0} \tag{3}$$

where $\mathbf{H}$ and $\mathbf{G}$ are the coefficient matrices obtained by integration over the boundary elements of the fundamental solution $\mathbf{t}^*$ and $\mathbf{u}^*$, respectively, times the corresponding shaped functions for the element type used, and $\mathbf{u}$ and $\mathbf{t}$ are the displacement and traction boundary nodal value vectors, respectively. This approach is especially advantageous in the numerical analysis of the foundation rock because the radiation conditions are intrinsically taken into account for unbounded domains such as this one, and only a limited extension of the free surface of the terrain around the structure needs to be discretized in order to obtain accurate results. More details can be found in Domínguez [37].

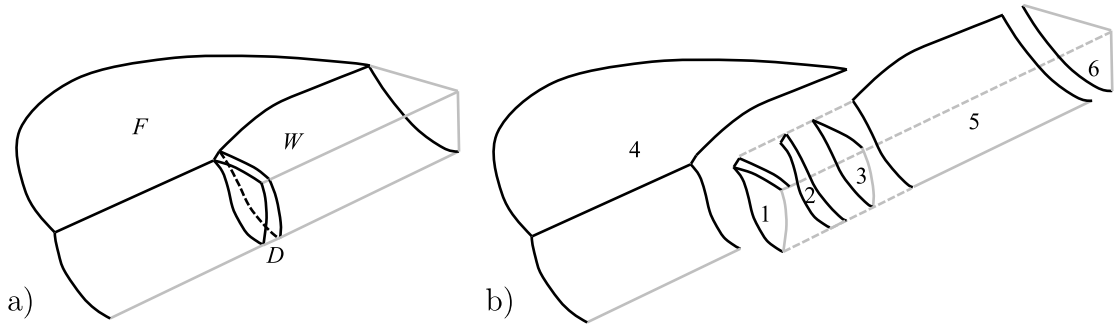

Fig. 3. (a) Idealized representation of the dam–foundation–reservoir system. (b) Detail of individual boundaries.

3.2. Reservoir near-field

As usual in this type of models, the water domain is represented as an inviscid fluid under small amplitude motions through the Helmholtz equation

$$\nabla^2 p + \left(\frac{\omega}{c}\right)^2 p = 0 \tag{4}$$

where $p(x, y, z, \omega)$ is the scalar field of hydrodynamic pressures and c is the wave propagation velocity. The geometry of the reservoir closest to the dam wall can be relevant for the dynamic analysis of the system. For this reason, the numerical model needs to be able to take such geometry into account. In this case, the boundary integral equation for the fluid domain can be written as

$$c^k p^k + \int_{\Gamma_w} \frac{\partial p^*}{\partial \mathbf{n}} p \, \mathrm{d}\Gamma_w - \int_{\Gamma_w} p^* \frac{\partial p}{\partial \mathbf{n}} \, \mathrm{d}\Gamma_w = 0 \tag{5}$$

where Γ_w represents the boundary of the reservoir; p^* is the half-space fundamental solution for the hydrodynamic pressures in the fluid domain for a harmonic punctual source pressure at collocation point $\mathbf{x}^k$ [37], with $p = 0$ at the surface of the water; c^k is the local free term at the same point; and $\mathbf{n}$ is the unit normal vector along Γ_w. After the discretization of the reservoir contour (with the exception of the surface of the water), Eq. (5) can be written for all nodes in Γ_w, which allows to express the relationship between the hydrodynamic pressures nodal values $\mathbf{p}$ and its derivatives $\mathbf{q}$ as

$$\mathbf{H}^w \mathbf{p} - \mathbf{G}^w \mathbf{q} = \mathbf{0} \tag{6}$$

where $\mathbf{G}^w$ and $\mathbf{H}^w$ are the coefficient matrices obtained by integration over the boundary elements of the scalar fundamental solution, and its flux, times the corresponding shaped functions for the element type used.

3.3. Excitation model

The dam–foundation–reservoir system will be assumed to be subjected to a seismic excitation defined by vertically-incident time–harmonic planar shear waves. Under this situation, the fields of displacements and tractions in the region where the seismic action originates can be expressed as the superposition of the incident field and the diffracted field, and Eq. (3) must be understood to be written in the diffracted field. Thus, the equation for the foundation rock can be written as

$$\mathbf{H}^F \mathbf{u}^F - \mathbf{G}^F \mathbf{t}^F = \mathbf{H}^F \mathbf{u}_{ff} - \mathbf{G}^F \mathbf{t}_{ff} \tag{7}$$

where $\mathbf{u}^F$ and $\mathbf{t}^F$ are the nodal values of the total displacements and traction fields in the foundation rock region, and $\mathbf{u}_{ff}$ and $\mathbf{t}_{ff}$ are the well-known closed-form displacement and traction components of the incident field in a half-space [38,39].

3.4. Coupled system synthesis. Boundary conditions, compatibility and equilibrium equations

The final linear system of equations to be solved is built by applying equilibrium and compatibility conditions between the different regions involved. In order to present such system of equations, let us denote the three domains and six boundaries and interfaces as illustrated in Fig. 3. Thus, Eqs. (3), (6) and (7), for dam (D), rock foundation (F) and water (W) regions, respectively, can be partitioned as

$$\mathbf{H}_1^D \mathbf{u}_1^D + \mathbf{H}_2^D \mathbf{u}_2^D + \mathbf{H}_3^D \mathbf{u}_3^D - \mathbf{G}_1^D \mathbf{t}_1^D - \mathbf{G}_2^D \mathbf{t}_2^D - \mathbf{G}_3^D \mathbf{t}_3^D = \mathbf{0} \tag{8a}$$

$$\mathbf{H}_2^F \mathbf{u}_2^F + \mathbf{H}_4^F \mathbf{u}_4^F + \mathbf{H}_5^F \mathbf{u}_5^F - \mathbf{G}_2^F \mathbf{t}_2^F - \mathbf{G}_4^F \mathbf{t}_4^F - \mathbf{G}_5^F \mathbf{t}_5^F = \mathbf{H}^F \mathbf{u}_{ff}^F - \mathbf{G}^F \mathbf{t}_{ff}^F \tag{8b}$$

$$\mathbf{H}_3^W \mathbf{p}_3 + \mathbf{H}_5^W \mathbf{p}_5 + \mathbf{H}_6^W \mathbf{p}_6 - \mathbf{G}_3^W \mathbf{q}_3 - \mathbf{G}_5^W \mathbf{q}_5 - \mathbf{G}_6^W \mathbf{q}_6 = \mathbf{0} \tag{8c}$$

On the other hand, the boundary conditions, and the equilibrium and compatibility equations that relate dynamic and kinematic variables along the interfaces shared by two different regions are

$$\mathbf{t}_1^D = \mathbf{0} \quad ; \quad \mathbf{t}_4^F = \mathbf{0} \tag{9a}$$

$$\mathbf{t}_2^D + \mathbf{t}_2^F = \mathbf{0} \quad ; \quad \mathbf{u}_2^D = \mathbf{u}_2^F \tag{9b}$$

$$\mathbf{t}_3^D + \mathbf{p}_3 \mathbf{n}^D = \mathbf{0} \quad ; \quad \mathbf{q}_3 + \rho_w \omega^2 \mathbf{u}_3^D \mathbf{n}^D = \mathbf{0} \tag{9c}$$

$$\mathbf{t}_5^F + \mathbf{p}_5 \mathbf{n}^F = \mathbf{0} \quad ; \quad \mathbf{q}_5 + \rho_w \omega^2 \mathbf{u}_5^F \mathbf{n}^F = \mathbf{0} \tag{9d}$$

$$\mathbf{q}_6 + \mathbf{M} \mathbf{p}_6 = \mathbf{0} \tag{9e}$$

where Eq. (9a) represents the free-surface boundary conditions, Eqs. (9b) to (9d) represent equilibrium and compatibility equations at the dam-abutment (Γ_2), dam-upstream face (Γ_3) and reservoir–rock (Γ_5) interfaces, and Eq. (9e) represents the transmitting boundary condition at the truncated boundary of the reservoir (Γ_6), as described below in Section 3.5, where matrix $\mathbf{M}$ is also defined. Here, $\mathbf{n}^F$ and $\mathbf{n}^D$ are the unit normal vectors to boundaries of the rock–foundation and dam, respectively. The application of these conditions to the BEM Eqs. (8) yields a linear system of equations of the type $\mathbf{A}\mathbf{x} = \mathbf{b}$ where matrix $\mathbf{A}$ is defined in Eq. (10) (see Box I),

$$\mathbf{x} = \begin{pmatrix} \mathbf{u}_1^D & \mathbf{u}_2^F & \mathbf{u}_3^D & \mathbf{t}_2^F & \mathbf{u}_4^F & \mathbf{u}_5^F & \mathbf{p}_3 & \mathbf{p}_5 & \mathbf{p}_6 \end{pmatrix} \tag{11}$$

and

$$\mathbf{b} = \begin{pmatrix} \mathbf{0} \\ \mathbf{H}^F \mathbf{u}_{ff}^F - \mathbf{G}^F \mathbf{t}_{ff}^F \\ \mathbf{0} \end{pmatrix} \tag{12}$$

This system allows to compute the unknown displacements, tractions and pressures along all nodes defined at all boundaries and interfaces of the problem, for each frequency ω. The implementation of this synthesis process can be a complex task in which many particular situations that depend on the problem must be taken into account. The application of techniques where the unknowns are duplicated in common nodes between interfaces and where the collocation is done as many times as different boundaries are present, facilitates and

$$\mathbf{A}=\begin{bmatrix} \mathbf{H}_1^D & \mathbf{H}_2^D & \mathbf{H}_3^D & \mathbf{G}_2^D & \mathbf{0} & \mathbf{0} & \mathbf{G}_3^D\mathbf{n}^D & \mathbf{0} & \mathbf{0} \\ \mathbf{0} & \mathbf{H}_2^F & \mathbf{0} & -\mathbf{G}_2^F & \mathbf{H}_4^F & \mathbf{H}_5^F & \mathbf{0} & \mathbf{G}_5^F\mathbf{n}^F & \mathbf{0} \\ \mathbf{0} & \mathbf{0} & \rho_w\omega^2\mathbf{G}_3^W\mathbf{n}^D & \mathbf{0} & \mathbf{0} & \rho_w\omega^2\mathbf{G}_5^W\mathbf{n}^F & \mathbf{H}_3^W & \mathbf{H}_5^W & \mathbf{H}_6^W+\mathbf{G}_6^W\mathbf{M} \end{bmatrix} \tag{10}$$

Box I.

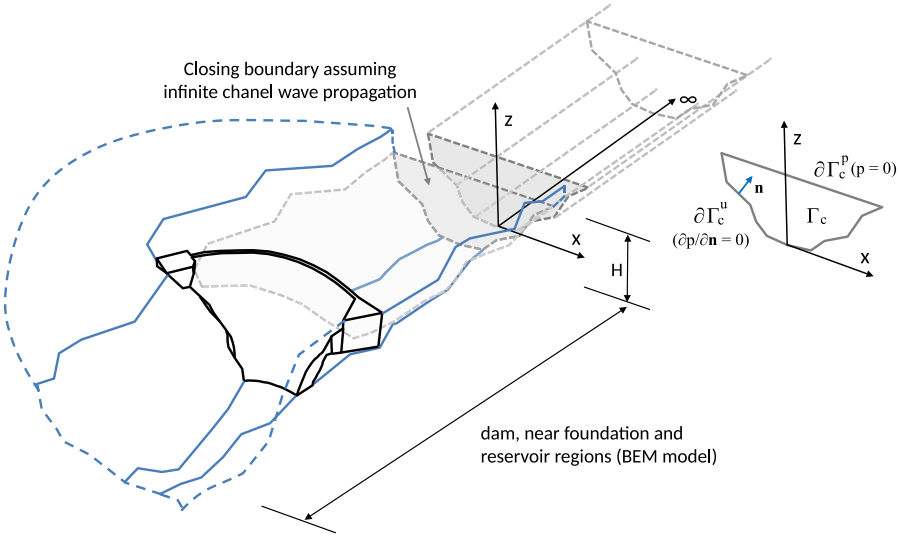

Fig. 4. Near-field model and transmitting boundary representing an infinite open channel with constant geometry.

generalizes this procedure with a very small relative increase in the size of the system of equations. In addition, these techniques, combined with non-nodal collocation strategies, allows the effective treatment of points where flow or tension may be undefined (corner problem). For more details see [40,41].

3.5. Reservoir far-field. Definition of the transmitting boundary

Section 3.2 addressed the treatment of the portion of the reservoir that is closest to the dam wall, which is modeled in detail. A detailed model of the portions of the reservoir that are more distant from the dam wall is less relevant. For this reason, the far-field reservoir is usually simplified by specific boundary conditions set at a truncated boundary placed far enough from the points of interest in the study. There exist different alternatives to define such boundary conditions, which in any case must be able to represent the radiation of energy away from the reservoir through that channel.

In order to define an adequate transmitting boundary condition at the truncated end of the reservoir for the problem at hand, this section will first define a set of alternatives, and will then evaluate and compare them. A rigorous semi-analytical solution for the problem of an infinite open channel with a generic geometry of the channel cross-section will be presented first, and will be used later as a reference solution. The two less complex radiation conditions by Sommerfeld and Humar and Roufaiel will be presented later. A benchmark problem will be then briefly studied in order to evaluate the more adequate boundary condition to be used for the analysis of the reservoir at hand.

3.5.1. Rigorous semi-analytical solution for an infinite open channel with generic geometry cross-section

Thus, assuming an infinite open channel with constant geometry beyond the truncated boundary is a common technique (see, for instance, Hall and Chopra [42] or Domínguez and Maeso [5]). This assumption allows to set a semi-analytical solution for the propagation of the hydrodynamic waves along the channel, and the formulation, therefore, of the equations of a transmitting boundary that models rigorously this situation.

Let us then consider an infinite channel whose bottom and walls are perfectly reflectant. The solution for the field of hydrodynamic pressures in this channel must verify the Helmholtz equation (4) considering $p=0$ on $\partial\Gamma_c^p$ and $\partial p/\partial\mathbf{n}=0$ on $\partial\Gamma_c^u$ (see Fig. 4). Considering a solution of the type

$$p=\boldsymbol{\Phi}(x,z)\mathrm{e}^{-Ky} \tag{13}$$

where K is the wave number, the solution of Eq. (4) by separation of variables yields the following eigenvalue problem in Γ_c

$$\nabla^2\boldsymbol{\Phi}+\lambda^2\boldsymbol{\Phi}=0 \tag{14}$$

where $\boldsymbol{\Phi}$ are the resulting eigenvectors, and λ the eigenvalues, whose solution is of the type $\lambda^2=K^2+(\omega/c)^2$. The resolution of Eq. (14) yields λ_m and $\boldsymbol{\Phi}_m$ for each mode m, being the wave number K_m for each node represented by

$$K_m=\sqrt{\lambda_m^2-\left(\frac{\omega}{c}\right)^2} \tag{15}$$

A general complete solution can now be written as the superposition of all modes as

$$p=\sum_{m=1}^{\infty}A_m\boldsymbol{\Phi}_m\mathrm{e}^{-K_m y} \tag{16}$$

where A_m are the participation factors of each mode, initially unknown, and dependent of the specific configuration. As in other problems of this kind, the properties of the propagation modes in the channel depend on the sign of the radicand in Eq. (15). Thus, if the radicand is positive, then $K_m\in\mathbb{R}^+$, and the exponential term decays with distance, which means that such modes damp away fast and are not relevant far from the origin of the perturbation. On the contrary, if the radicand is negative, then $K_m\in\mathbb{I}^+$, resulting in modes that propagate along the channel without decaying which imply that they need to be taken

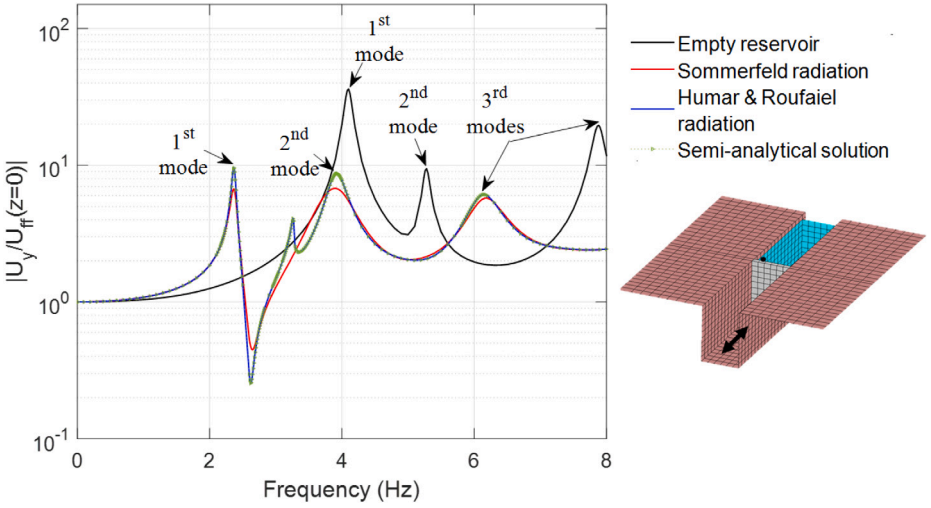

Fig. 5. Frequency response functions of a planar dam wall in a rectangular cross-section infinite canyon, subject to vertically-incident shear waves, with different types of transmitting boundary conditions at the truncated end of the reservoir.

considered in order to properly simulate the radiation of this energy out of the model.

Eq. (16), and its derivative, can be taken as the starting point to derive a rigorous radiating boundary condition in the nodes of a planar closing boundary of the reservoir at coordinate $y = 0$. There are explicit solutions (exacts or approximate) for some specific geometries of the channel cross-section (see, for instance, [21,43,44]) but, for a generic geometry, the solution will be semi-analytical, as the eigenvalue problem stated in Eq. (14) shall be solved numerically. In any case, once the eigenvalues and eigenmodes are known, the finite expansion of the hydrodynamic pressures and their derivatives can be computed for each node i from Eq. (16). Given that $y = 0$ in the chosen reference system, the vectors $\mathbf{p}$ and $\mathbf{q}$ that gather the pressures and their derivatives at every node of the closing boundary can be written in matrix form as

$$\mathbf{p} = \mathbf{\Phi A} \tag{17}$$

$$\mathbf{q} = -\mathbf{\Phi K A} \tag{18}$$

where $\mathbf{\Phi}$ is the matrix that gathers all eigenvectors, $\mathbf{A}$ is the vector of participation factors and $\mathbf{K}$ is a diagonal matrix with all wave numbers. Thus, taking into account that $\mathbf{\Phi}$ is an orthogonal matrix, the expression for the radiation condition at the nodes can be obtained from Eqs. (17) and (18) as

$$\mathbf{q} + \mathbf{M}\mathbf{p} = \mathbf{0} \tag{19}$$

where $\mathbf{M} = \mathbf{\Phi K \Phi}^{-1}$.

3.5.2. Truncated radiation condition for the first mode of the channel

In most real situations, only a very small number of eigenvalues are located within the frequency range of interest due to the dimensions of usual problems and the large spacing between modes. Consequently, the expansion (16) will consist of only a few meaningful terms. In fact, in many cases, including only the first natural frequency can be enough, as proposed by Humar and Roufaiel [17], which allows to simplify Eq. (19) for each node i to

$$\left(\frac{\partial p}{\partial y}\right)_i + \sqrt{\lambda_1^2 - \left(\frac{\omega}{c}\right)^2}\, p_i = 0 \tag{20}$$

which is a Robin condition, uncoupled for each node of the boundary, and straightforward to incorporate in any numerical code. For rectangular narrow channels, the first mode is related to the water depth H, being $\lambda_1 = \pi/2H$.

3.5.3. Sommerfeld radiation condition

For values of $\omega/c \gg \lambda_1$, Eq. (20) collapses into the well-known Sommerfeld radiation condition for 1D problems (see for instance Eringen and Suhubi [45]):

$$\left(\frac{\partial p}{\partial y}\right)_i + \mathrm{i}\left(\frac{\omega}{c}\right) p_i = 0 \tag{21}$$

where $\mathrm{i} = \sqrt{-1}$ is the imaginary unit. This is a classical Robin condition widely used in elastodynamics due to its simplicity and whose application to model this effect will also be explored in this work.

3.5.4. Benchmark problem

These alternative formulations for the transmitting boundary condition at the truncated end of the reservoir were implemented in the multidomain Boundary Element Method (BEM) code in the frequency domain described in Maeso et al. [7,8]. The results computed using these formulations will be studied and compared here for a simplified model of the dam–foundation–reservoir: a planar dam wall with the same height as Soria arch dam (120 m) and average length and width of 80 and 10 m, respectively, completely embedded in a prismatic canyon with rectangular cross-section, as illustrated in Fig. 5. The properties for dam wall, rock foundation and water region are those defined in Table 2. The depth of the water in the reservoir is defined as $H = 110$ m. For this case of a rectangular channel, the eigenvalue and eigenfrequencies for the open channel are explicit (see, for instance, Domínguez and Maeso [6] or Weber [44]), and can be easily derived. The fundamental frequency of the channel is $f_1 = 3.2$ Hz. The system is subject to vertically-incident shear waves that produce motions along the axis of the channel.

Fig. 5 presents the response of a point located at the top of the dam wall for the three different alternative boundary conditions and for the empty reservoir situation. The significant reduction in the natural frequencies of the dam wall, due to the presence of the water, is clear. Under full-reservoir conditions, the response at the dam wall below the first mode of the wall is insensitive to the boundary condition. Sommerfeld radiation condition provides an overdamped response in a wide range of frequencies, especially around the first and second modes of the wall, and around f_1, which is marked with a clear peak in the frequency response function computed with both the semi-analytical and Humar and Roufaiel's transmitting boundaries. However, as mentioned in Section 3.5.2, for frequencies $f \gg f_1$, the solution obtained considering Sommerfeld's condition converges with the response computed considering the semi-analytical radiation condition as described in Eq. (19). At the same time, Humar and Roufaiel's radiation

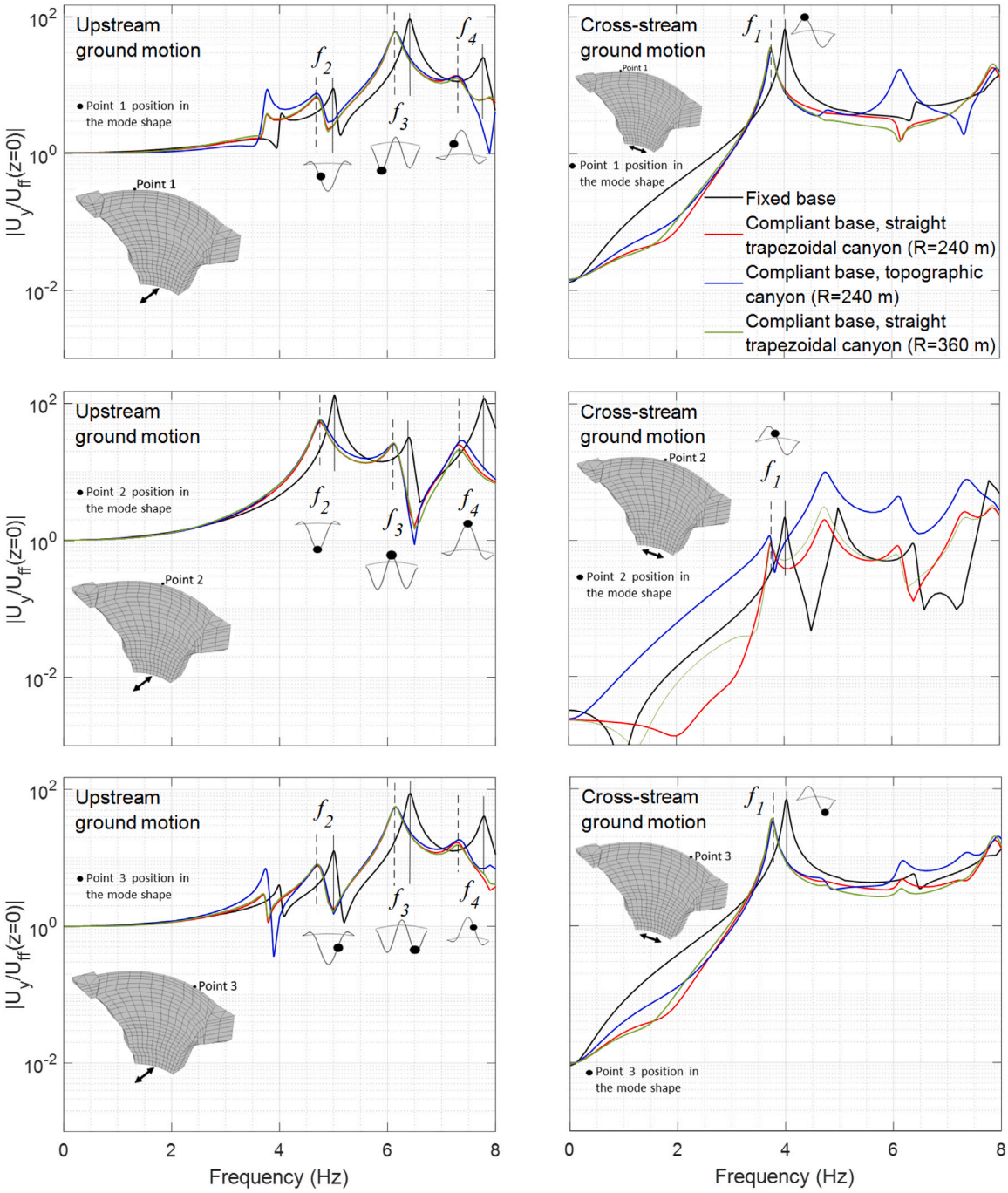

Fig. 6. Frequency response functions at the dam crest for fixed and compliant-base dam models and the different representations of the canyon. Responses are shown at point 1 (upper plots), point 2 (middle plots) and point 3 (bottom plots).

condition matches perfectly that rigorous semi-analytical solution for all the frequency range of interest, as the second frequency of the channel is above nine Hz. For this reason, given its precision, efficiency and simplicity, Humar and Roufaiel's radiation condition will be used later for the study of the response of Soria arch dam.

4. Results

4.1. Influence of DSSI and canyon geometry modeling on the dynamic response of the dam in empty reservoir conditions

In order to quantify the influence of the dynamic soil–structure interaction and of the geometry of the canyon on the dynamic response of the dam in empty reservoir conditions, Fig. 6 presents the frequency response functions at different points along the dam crest for different situations. The response of the system under upstream (left column) and cross-stream (right column) incident ground motions is plotted for points 1, 2 and 3 (as defined in Fig. 1b) in the upper, middle and bottom rows, respectively. In the case of the fixed-base system, the excitation is defined as a harmonic uniform unitary displacements field along the abutments. Each of the plots presents the responses obtained for fixed and compliant-base configurations, and for the three models of the canyon.

DSSI influences very clearly the natural frequencies of the system despite the significant stiffness of the rock and the relatively short span of the dam wall in comparison with its height. Table 3 presents

Table 3
Comparison between natural frequencies for fixed-base and the different compliant-base models. The reduction in the natural frequency with respect to fixed-base conditions is shown in parentheses.

	First mode	Second mode	Third mode	Fourth mode
Fixed base	4.01 Hz	5.02 Hz	6.42 Hz	7.80 Hz
Compliant base trapezoidal canyon ($R = 2H$)	3.79 Hz (−5.48%)	4.77 Hz (−4.98%)	6.16 Hz (−4.05%)	7.46 Hz (−4.35%)
Compliant base topographic canyon ($R = 2H$)	3.80 Hz (−5.23%)	4.78 Hz (−4.78%)	6.17 Hz (−3.89%)	7.47 Hz (−4.23%)
Compliant base trapezoidal canyon ($R = 3H$)	3.78 Hz (−5.73%)	4.76 Hz (−5.18%)	6.16 Hz (−4.05%)	7.46 Hz (−4.35%)

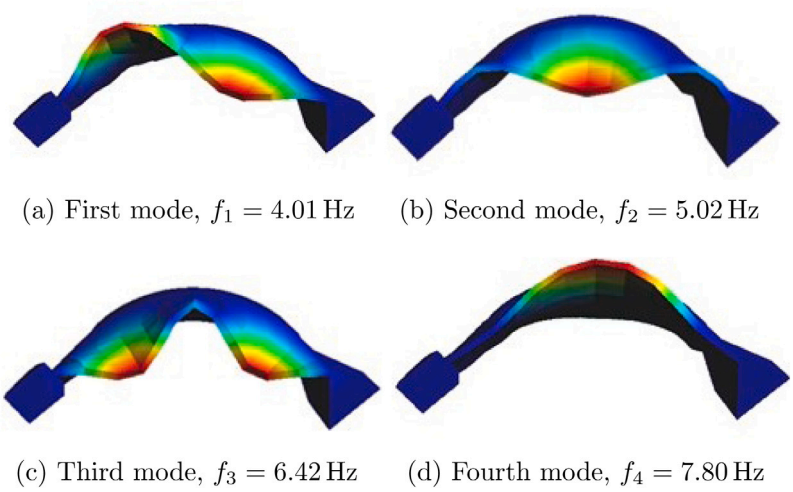

Fig. 7. Natural frequencies and mode shapes of the dam wall under fixed-base condition.

the comparison between the natural frequencies corresponding to the fixed-base and the different compliant-base models, together with the quantification of the reduction in frequency produced by the soil–structure interaction. Here, natural frequencies are determined as the frequencies of the peaks of the imaginary parts of each frequency response function. This reduction is, in average, of 5.5%. 5.0%, 4.0% and 4.3% for the first, second, third and forth natural frequencies, respectively,with insignificant differences among the different models of canyon. The different peaks in the frequency response functions have been labeled in order to identify the corresponding specific mode of vibration for each one of them. Thus, the natural frequencies are marked in each plot by means of solid and dashed lines for the fixed and complaint base cases, respectively. Symbols f_1, f_2, f_3 and f_4 are used to denote the first, second, third and fourth natural frequencies, respectively. As expected, the fundamental mode (asymmetric) can be observed clearly under cross-stream excitation (case in which, in turn, symmetrical modes can hardly be observed), while the second, third and fourth modes (symmetric) are evident in the frequency response functions computed from upstream excitation. Fig. 7 presents the first four mode shapes of vibration, which are also depicted inside Fig. 6 for reference. This modal shapes agree with the usual shapes for this type of structures, as shown, for instance, by Hariri-Ardebili et al. [26].

On the other hand, soil–structure interaction tends also to imply, as expected, a reduction in the response recorded at the dam crest due to material and radiation damping through the rock. This is always true when straight trapezoidal canyons are considered but, when the topographic canyon is employed, some increases are observed in the responses. More precisely, the amplitude of the response around the first natural frequency of the dam increases significantly in points 1 and 3 for upstream incident ground motion, and the amplitudes of the response between 4.1 Hz and 7.9 Hz also increase very importantly in point 2 for cross-stream incident ground motion. It is also worth noting that considering a simplified straight trapezoidal geometry of the canyon instead of its actual topographic geometry has some influence on the amplitude of the dynamic response at certain points in some frequency ranges, mostly under cross-stream incident excitation but also in the upstream direction. However, the influence on the observed natural frequencies is insignificant, which allows to employ the trapezoidal canyon models in the next sections for the study of the evolution of the natural frequencies. In any case, it is worth highlighting that these conclusions regarding the limited influence of the reservoir geometry on the dynamic response of the dam apply to the specific quasi–symmetrical dam studied here, while a larger influence is expected in more asymmetrical cases.

On the other hand, when assessing the adequacy of the chosen extension for these straight canyon meshes, it has been shown that increasing the mesh extension beyond $R = 2H$ does not influence significantly the results. For these reasons, the mesh with a straight trapezoidal canyon and $R = 2H$ is used in the following sections.

4.2. Influence of the radiation condition modeling at the truncated end of the reservoir

Section 3.5 presented alternative formulations for the transmitting boundary condition at the truncated end of the reservoir, and compared them in a simplified benchmark problem, reaching the conclusion that the simplified Humar and Roufaiel's radiation condition provides an accurate response. The benchmark problem consisted of a rectangular channel, differently from the simplified model of Soria's reservoir, that features an isosceles prismatic cross-section in the channel, that represents better the actual geometry of the site.

The fundamental frequency to be used in Eq. (20) is a function of the geometry of the channel and, mainly, of the water level. In trapezoidal narrow canyons, an approximate value of this frequency can be computed using the solutions proposed by Shul'man [43] but whose exact value has to be calculated by numerically solving the eigenvalue

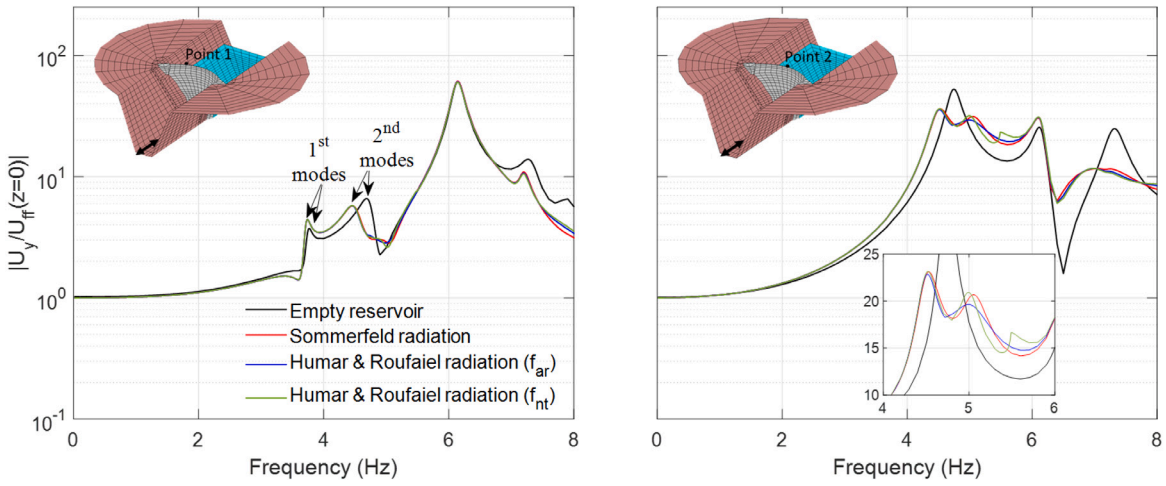

Fig. 8. Frequency response functions at the dam crest for compliant-base dam model and the different boundary conditions at the truncated boundary of the reservoir. Responses are shown at point 1 (left plot) and point 2 (right plot). $H = 76$ m.

problem represented by Eq. (14). Since the depth of the water reservoir is the most determining variable in this calculation, it can also be useful to assess whether the explicit solution of the rectangular channel ($\lambda_1 = \pi/2H$) can be used as an eigenvalue for this problem. Thus, the influence of adopting such simplified expression for the fundamental frequency, or its rigorous value, is briefly investigated in this section for the problem at hand. Sommerfeld's radiation condition is also included in order to show the influence of the different conditions in this more realistic configuration.

Thus, Fig. 8 presents the frequency response functions for the displacements at the dam crest with respect to the free-field seismic displacements produced by the vertically-incident upstream shear waves, for $H = 76$ m. The analytical fundamental frequency for a channel with rectangular cross-section of this depth is $f_{ar} = 4.73$ Hz, while the numerical fundamental frequency for the channel with the actual straight trapezoidal cross-section is $f_{nt} = 5.48$ Hz. The response is shown for two different points along the dam crest. In this more realistic model of the dam–foundation–reservoir system, the influence of the transmitting boundary condition is even less important than in the previous benchmark case. At point 1, the differences between the three tested models are negligible. At the mid point of the crest (point 2), some differences can be found between 4.5 and 6 Hz, especially at $f \simeq f_{nt}$, depending on the value of the fundamental frequency adopted for the Humar-Roufaiel model (f_{ar} or f_{nt}). Therefore, the results presented in the next section are computed with the most accurate solution among these three, i.e., Humar and Roufaiel's radiation condition with numerically computed fundamental frequencies for the trapezoidal cross-section with the corresponding water depths for each case.

4.3. Influence of water level and SSI on the dynamic response of the dam

The objective of this section is twofold: on the one hand, it studies how the variations in the height of the water held by the dam influences the dynamic response of the dam wall; and in the other hand, it also addresses the question of how relevant is SSI in this case. To do so, the dynamic response of the system has been studied under five different levels of water in the reservoir (0, 30, 50, 76 and 112 m) corresponding to ratios of 0%, 25%, 42%, 63% and 93% of the total height of the wall. As stated above, a straight trapezoidal canyon, with $R = 2H$ is employed, and Humar and Roufaiel's radiation condition is stated at the truncated boundaries. The needed eigenvalues corresponding to the channel are computed numerically, yielding the following fundamental frequencies: $f_1(H = 30) = 12.87$ Hz, $f_1(H = 50) = 7.97$ Hz, $f_1(H = 76) = 5.48$ Hz and $f_1(H = 112) = 3.86$ Hz. Fig. 9 presents the displacements in the upstream direction at two different points of the dam crest, for fixed-base and compliant-base models. In the first model, the system is subject to harmonic uniform unitary displacements field along the abutments in the upstream direction, while in the second model, vertically-incident shear waves produce unitary ground surface free-field displacements, in the same direction.

The first mode, mostly asymmetric, is only captured at point 3, which is located in a side, and is not observed in the response at point 2. On the other hand, the fundamental frequencies of the channel appear very clearly in the functions, especially at point 3 for the fixed base case. These frequencies are not so clearly apparent in the results obtained with the complete model including the rock foundation region because of its higher damping and capacity to absorb the waves along the near channel–rock interfaces. When the level of the reservoir is very low ($H = 30$ m, 25% of the maximum height), the response of the dam wall is basically unaltered with respect to the empty-reservoir case, in all the analyzed frequency range. When the level of the reservoir raises to $H = 50$ m (just below 50% of the height), the response of the dam wall is only affected for $f > 6.4$ Hz. For reservoir levels above these values, the response of the system is altered along the whole frequency range. As expected, the values of the natural frequencies of the different modes tend to decrease with the depth of the reservoir. For $H = 76$ m, the natural frequencies decrease slightly, while for $H = 112$ m, all of them decrease significantly with respect to the ones obtained with the other three water depths studied. The response for these high levels of water do not show a clear peak for a forth mode. The influence of the dynamic soil–structure interaction is seen very clearly in Fig. 9, where not only the natural frequencies are moved towards lower frequencies when the flexibility of the foundation rock is taken into account (as already seen in Section 4.1), but also the level of damping in the system is significantly increased, leading to lower amplitudes in the response of the system.

Fig. 10 presents the evolution of the natural frequencies with the depth of the water in the reservoir, computed for the complete dam–reservoir–foundation rock system. The trends mentioned above are more clearly visualized here, and are in line with the results found experimentally by other authors such as Pereira et al. [31].

4.4. Experimental results

In order to evaluate the ability of the proposed numerical model to represent the dynamic response of the system under low-level vibrations, a short experimental campaign was carried out on the dam on 27th June 2022, at a moment when the reservoir was almost empty. Unfortunately, and due to the lack of rains, it has not been possible to

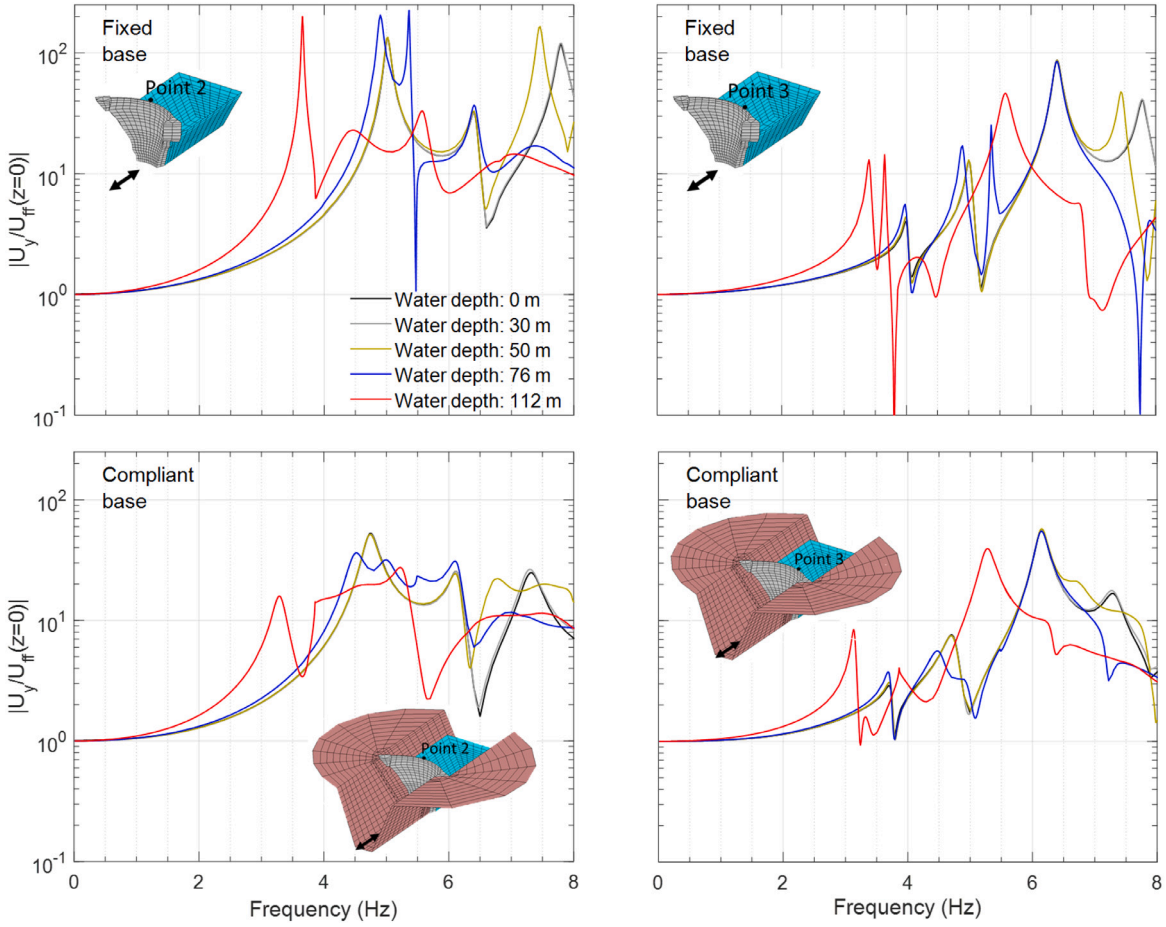

Fig. 9. Dynamic response of the dam wall for different water depths behind the dam, considering fixed and complaint-base conditions.

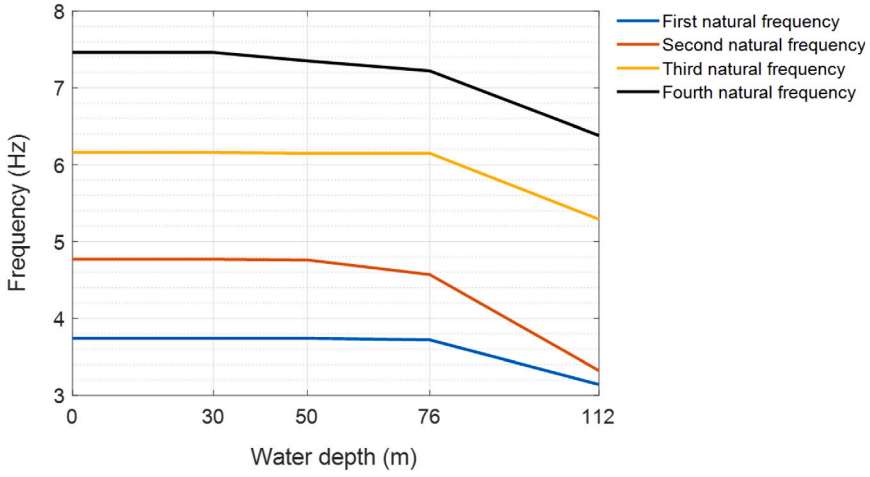

Fig. 10. Evolution of the first and second natural frequencies with reservoir level.

measure the response of the dam with any significant amount of water. Ambient vibration tests were carried out, being worth highlighting that the dam is located far from any relevant populations or roads, in a valley where wind is also usually very weak, so very low levels of ambient excitations are expected. Two Tromino® Blu velocimeters were employed to measure the response of the structure at eight points, P1 to P8 (see Fig. 11), along the dam crest, with a spacing between stations of approximately 20 m. One of the sensors was placed at a fixed position at P6 and used as reference, while the second unit was used as moving sensor along the other seven positions, recording the vibrations of the dam wall during 10 min at each location, and with synchronization via GPS. A sampling rate of 512 Hz was employed. The sensors were always oriented so that one channel was perpendicular to the mid line of the dam crest.

The multi-dataset pre-scaled Frequency Domain Decomposition (FDD) [46,47] and the Peak–Picking (PP) [48] methods are used, with the first singular values of the PSD matrix computed through the former employed for identification of the structural natural frequencies with the latter. Peaks that were found to be associated to non-structural origins, such as the fundamental frequency of the lamp posts along

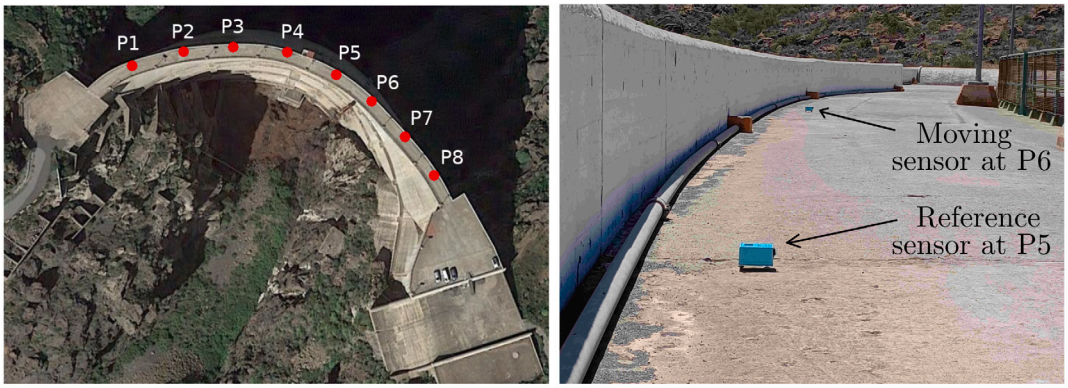

Fig. 11. (a) Sensor positions along the dam crest, (b) Detail of the sensors measuring at points P5 and P6.

Table 4
Comparison between experimental and numerical frequencies. Original and updated properties. f_{AV} and ξ_{AV} denote natural frequencies and damping ratios estimated from ambient vibration results, while ϵ denotes the error between numerical and experimental results.

Mode	Experimental results		Original properties		Updated properties	
	f_{AV} (Hz)	ξ_{AV} (%)	f_{BEM} (Hz)	ϵ (%)	f_{BEM} (Hz)	ϵ (%)
1	3.65	1.1	3.77	3.28	3.65	0.00
3	5.87	3.5	6.15	4.77	5.95	1.36

Table 5
MAC values between experimental and numerical mode shapes. Primatic canyon mesh.

	$\phi_{e,1}$ (3.65 Hz)	$\phi_{e,3}$ (5.87 Hz)
$\phi_{n,1}$ (3.65 Hz)	**0.9901**	0.0089
$\phi_{n,3}$ (5.95 Hz)	0.0229	**0.9032**

the dam crest, and frequencies associated to the pumps and pipes (see f_l and f_p, respectively, in Fig. 12) were discarded. In addition, the mode shapes of the remaining candidate structural natural frequencies were investigated, and those that presented feasible modal shapes were finally selected.

The analysis of the ambient vibrations experimental results allowed to identify clearly modes 1 and 3, whose estimated natural frequencies and modal damping ratios are presented in Table 4 (columns f_{AV} and ξ_{AV}, respectively) together with the corresponding natural frequencies computed from the complete boundary element model described above for the empty reservoir (column f_{BEM}, with original properties). Here, natural frequencies are determined as the frequencies of the peaks of the modulus of each frequency response function in order to allow a direct comparison with the frequencies estimated from the first singular values of the PSD matrix. The corresponding identified mode shapes are shown in Fig. 13, and are discussed below.

Even though generic properties for the foundation rock, and the available properties for the concrete in the dam wall, were employed for the numerical analysis, the agreement between numerical and experimental natural frequencies is high, with the maximum error, of around 5%, found for the third mode, as shown in the columns of the table for the results obtained with the original properties. In view of these results, the dam wall shear modulus was slightly updated to match the first natural frequency, yielding an updated $G = 7.7$ GPa (5.6% lower than the original $G = 8.16$ GPa). This updated stiffness allows to match the first natural frequency, and leads to a significant reduction of the difference in the values of the third natural frequency, whose error ϵ is now below 1.5%, with the errors computed as $\epsilon = |f_{AV} - f_{BEM}| \cdot 100/f_{AV}$.

Fig. 12 shows a comparison between the normalized first singular values of the computed PSD matrix, and the Frequency Response Functions computed numerically, with updated properties, for points P2 (red line, cross-stream ground motion) and P4 (blue line, upstream ground motion) on the dam crest. As mentioned before, the peaks marked as f_l and f_p were proven to be associated to the frequencies of the lamp post and pumping station, respectively. Even though numerical and experimental plots are of different nature, the comparison allow to highlight the correspondence of the computed and measured natural frequencies. The peaks associated to the first and third natural frequencies can be clearly identified in both cases. The first natural frequency is very clearly present in the experimental spectra, and its position coincides with the first peak of the numerical FRF under cross-stream excitation. The position of the third numerical natural frequency is again very close to the corresponding peak from the experimental results. On the contrary, the second mode can be observed in the numerical FRFs, but is not evident from the experimental results, and the measured response above the third natural frequency is not correctly represented by the numerical FRFs.

Fig. 13 presents the comparison of the modal shapes computed from the numerical model (solid lines) and estimated from the ambient vibration measurements (hollow circles at the eight measurements locations). The shown numerical modal shapes correspond to the models with updated material properties, both considering the simplified trapezoidal mesh for the canyon, and the more elaborated topographic mesh. The agreement between numerical and experimental modal shapes is very good, especially in the case of the first mode, for which the numerical mode shape is almost independent of the mesh of the canyon. In the case of the third mode, it can be seen that the numerical modal shape computed considering the simplified trapezoidal canyon is mostly symmetrical, while the experimental modal shape shows a certain degree of asymmetry that is much better reproduced by the numerical modal shape obtained from the topographic model, which suggests that taking into account the asymmetry of the canyon is relevant for a more accurate representation of the modal shapes of the dam.

In order to quantify the agreements between numerical and experimental modal shapes, Tables 5 and 6 present the values of the Modal Assurance Criterion between the experimental modal shapes and the numerical modal shapes obtained from the prismatic and the topographic canyons, respectively. A very good correlation is found for both modes. In the case of the first mode, a MAC value of around 0.99 is found. In the case of the third mode, the MAC value improves from 0.903 to 0.925 when the results from the topographic canyon are considered.

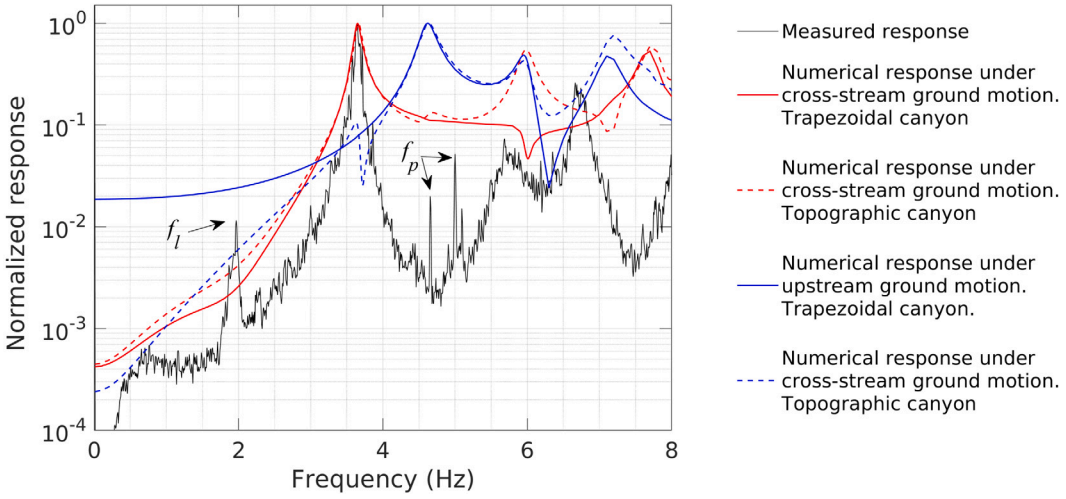

Fig. 12. Comparison between experimental (first singular values of the PSD from ambient vibrations) and numerical responses (Frequency Response Functions at points P2 (red) and P4 (blue) for trapezoidal and topographic models with updated properties). f_l and f_p denote the frequencies associated to the lamps, the pumps and the pipes.

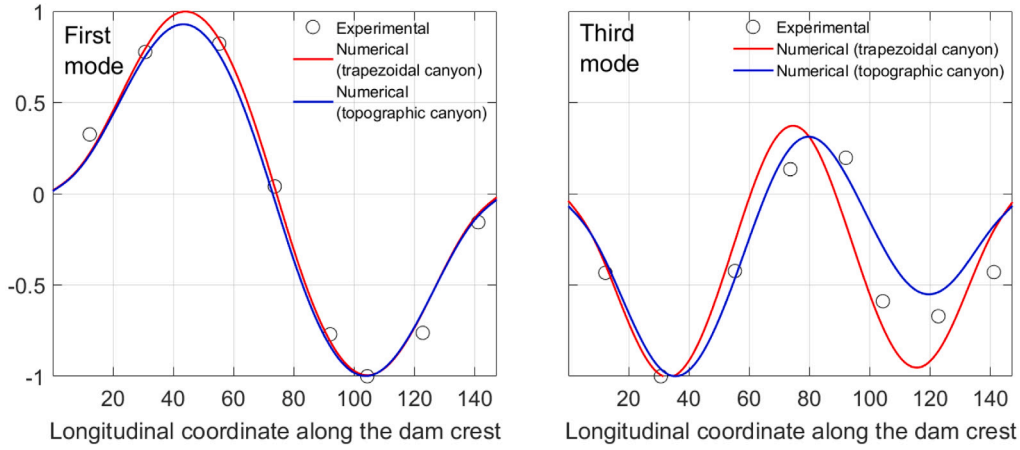

Fig. 13. Comparison between numerical and experimental modal shapes along the dam crest.

Table 6
MAC values between experimental and numerical mode shapes. Topographic canyon mesh.

	$\phi_{e,1}$ (3.65 Hz)	$\phi_{e,3}$ (5.87 Hz)
$\phi_{n,1}$ (3.65 Hz)	**0.9891**	0.0090
$\phi_{n,3}$ (5.98 Hz)	0.0556	**0.9254**

5. Conclusions

A BEM-based time–harmonic numerical model for the analysis of the dynamic characteristics of the Soria arch dam and reservoir under low-level vibrations, to be used in SHM applications, has been studied in this paper. The model is able to take into account the presence of the flexible rock foundation, the actual geometries of dam wall and reservoir, the different levels of the water held in the reservoir, the interaction between dam wall, rock and water in the reservoir, the incidence of vertically-incident far-field seismic waves, and the radiation of energy away of the system through such rock foundation unbounded domain and through the truncated boundary of the reservoir. The following conclusions have been drawn from the study:

- Dynamic Soil–Structure Interaction phenomena has a significant influence over the response of the system, both in empty-reservoir and full-reservoir conditions.
- As expected, dynamic Fluid–Structure Interaction also modifies dynamic response of the dam wall, although low levels (below 50%) of the water in the reservoir does not influence significantly the natural frequencies or modes.
- The consideration of Humar and Rouafiel's simplified radiation boundary condition at the truncated end of the reservoir, instead of a more rigorous transmitting boundary, has been shown to be able to produce accurate results for this specific problem. In fact, even Sommerfeld's radiation condition works significantly well. For this reason, Humar and Rouafiel's radiation boundary condition is adopted in the final complete proposal for the representation of the portion of the body of water that is not directly included in the model.
- Taking into account a simplified trapezoidal geometry for the canyon, instead of the actual topographic geometry of the canyon, does not produce a significant worsening of the results in terms of the estimation of the natural frequencies of the system.
- The proposed numerical model, in empty reservoir conditions, is tested by comparison against experimental ambient vibration tests. The first and third modes were clearly identified, while the second and fourth mode seems to be very weakly excited or highly damped. It is shown that the model is able to capture the natural frequencies identified in this experimental campaign, and only minor updates over the initially assumed material properties for the dam wall were needed to match, with a high level of accuracy,

the first and third natural frequencies. A high agreement is also reached between the mode shapes estimated from the experimental campaign and those computed using the proposed numerical model

- The numerical model built from the actual topographic geometry of the canyon is able to provide a better estimate of the modal shapes, at least for the third mode, when comparing with the experimentally obtained modes.
- The good correlation found between numerical and experimental natural frequencies and modal shapes for modes 1 and 3 suggests that the proposed model is able to represent the dynamic behavior of the dam wall under low-level vibrations, although the remaining modes could not be identified from the ambient vibration measurements. This was probably due to the low level of background excitation, but more work needs to be done in this regard in the future, in order to obtain a more complete experimental characterization of the structure.

For these reasons, the proposed numerical model is considered to be adequate for use in future studies of the dynamic behavior of the dam and, especially, in Structural Health Monitoring applications of the Soria arch dam through, for instance, the development of a Digital Twin [49,50] of the physical dam.

Declaration of competing interest

The authors declare that they have no known competing financial interests or personal relationships that could have appeared to influence the work reported in this paper.

Data availability

Data will be made available on request.

Acknowledgments

This research was partially supported by ACIISI, Spain–Gobierno de Canarias and European FEDER Funds Grant EIS 2021 04.

References

[1] Bukenya P, Moyo P, Beushausen H, Oosthuizen C. Health monitoring of concrete dams: a literature review. J Civ Struct Health Monit 2014;4:235–44.
[2] Fok KL, Chopra AK. Earthquake analysis of arch dams including dam-water interaction, reservoir boundary absorption and foundation flexibility. Earthq Eng Struct Dyn 1986;14:155–84.
[3] Fok KL, Chopra AK. Frequency response functions for arch dams: hydrodynamic and foundation flexibility effects. Earthq Eng Struct Dyn 1986;14:769–95.
[4] Tan H, Chopra AK. Earthquake analysis of arch dams including dam-water-foundation rock interaction. Earthq Eng Struct Dyn 1995;24:1453–74.
[5] Maeso O, Domínguez J. Earthquake analysis of arch dams I: Dam-foundation interaction. J Eng Mech 1993;119(3):496–512.
[6] Domínguez J, Maeso O. Earthquake analysis of arch dams II: Dam-water-foundation interaction. J Eng Mech 1993;119(3):513–30.
[7] Maeso O, Aznárez JJ, Domínguez J. Effects of space distribution of excitation on seismic response of arch dams. J Eng Mech 2002;128:759–68.
[8] Maeso O, Aznárez JJ, Domínguez J. Three dimensional models of reservoir sediment and effects on the seismic response of arch dams. Earthq Eng Struct Dyn 2004;33:1103–23.
[9] Aznárez JJ, Maeso O, Domínguez J. BE analysis of bottom sediments in dynamic fluid–structure interaction problems. Eng Anal Bound Elem 2006;30:124–36.
[10] García F, Aznárez JJ, Cifuentes H, Medina F, Maeso O. Influence of reservoir geometry and conditions on the seismic response of arch dams. Soil Dyn Earthq Eng 2014;67:264–72.
[11] García F, Aznárez JJ, Padrón LA, Maeso O. Relevance of the incidence angle of the seismic waves on the dynamic response of arch dams. Soil Dyn Earthq Eng 2016;90:442–53.
[12] Seghir A, Tahakourt A, Bonnet G. Coupling FEM and symmetric BEM for dynamic interaction of dam–reservoir systems. Eng Anal Bound Elem 2009;33(10):1201–10.
[13] Aftabi Sani A, Lotfi V. An effective procedure for seismic analysis of arch dams including dam-reservoir-foundation interaction effects. J Earthq Eng 2011;15(7):971–88.
[14] Li Z-Y, Hu Z-Q, Hong Z, Lin G. A novel scaled boundary finite element method for dynamic impedance of an arch dam foundation in a complex layered half–space. Eng Anal Bound Elem 2022;134(1):184–98.
[15] Concepción-Guodemar Y, Escuder-Bueno I, Morales-Torres A, Cervera-Miquel D. Numerical modeling for the design of monitoring in double–curvature arch dams for a change of use. Analysis for soria dam (Canary islands-Spain). In: 26th international congress on large dams, 2018. 2018, p. 1225–30.
[16] Rezaiee-Pajand M, Kazemiyan MS, Aftabi Sani A. A literature review on dynamic analysis of concrete gravity and arch dams. Arch Comput Methods Eng 2021;28:4357–72.
[17] Humar J, Roufaiel M. Finite element analysis of reservoir vibration. J Eng Mech 1983;109(1):215–30.
[18] Medina F, Domínguez J. Boundary elements for the analysis of the seismic response of dams including dam–water–foundation interaction effects. I. Eng Anal Bound Elem 1989;6(3):152–7.
[19] Medina F, Domínguez J. Boundary elements for the analysis of the seismic response of dams including dam–water–foundation interaction effects. II. Eng Anal Bound Elem 1989;6(3):158–63.
[20] Domínguez J, Meise T. On the use of the BEM for wave propagation in infinite domains. Eng Anal Bound Elem 1991;8(3):132–8.
[21] Szczesiak T, Weber B. Hydrodynamic effects in a reservoir with semi–circular cross–section and absorptive bottom. Soil Dyn Earthq Eng 1992;11:203–12.
[22] Jafari M, Lotfi V. Dynamic analysis of concrete gravity dam-reservoir systems by a wavenumber approach for the general reservoir base condition. Sci Iran 2018;25(6):3054–65.
[23] Mircevska V, Bickovski V, Aleksov I, Hristovski V. Influence of irregular canyon shape on location of truncation surface. Eng Anal Bound Elem 2013;37:624—636.
[24] Mircevska V, Nastev M, Hristovski V, Bulajic I. Arch dam-fluid interaction considering reservoir topology. Earthq Eng Struct Dyn 2014;14:155–84.
[25] Farzad R, Lotfi V. Modal analysis of concrete arch dam–reservoir–massed foundation system in frequency domain. In: Proceedings of the institution of civil engineers - structures and buildings; 2021, p. 1–13.
[26] Hariri-Ardebili MA, Mahdi Seyed-Kolbadi S, Saouma VE, Salamon JW, Nuss LK. Anatomy of the vibration characteristics in old arch dams by random field theory. Eng Struct 2019;179:460–75.
[27] Darbre GR, de Smet CAM, Kraemer C. Natural frequencies measured from ambient vibration response of the arch dam of mauvoisin. Earthq Eng Struct Dyn 2000;29:577–86.
[28] Darbre GR, Proulx J. Continuous ambient-vibration monitoring of the arch dam of Mauvoisin. Earthq Eng Struct Dyn 2002;31:475–80.
[29] Calcina SV, Eltrudis L, Piroddi L, Ranieri G. Ambient vibration tests of an arch dam with different reservoir water levels: experimental results and comparison with finite element modelling. Sci World J 2014;2014.
[30] García-Palacios JH, Soria JM, Díaz IM, Tirado-Andrés F. Ambient modal testing of a double-arch dam: The experimental campaign and model updating. In: Journal of physics: conference series, Vol. 744. IOP Publishing; 2016, 012037.
[31] Pereira S, Magalhães F, Gomes JP, Cunha A, Lemos JV. Vibration-based damage detection of a concrete arch dam. Eng Struct 2021;235:112032.
[32] Guo X, Dufour F, Humbert N. Modal analysis of an arch dam combining ambient vibration measurements, advanced fluid–element method and modified engineering approach. Earthq Eng Struct Dyn 2022;51(6):1321–42.
[33] Pereira S, Magalhães F, Cunha A, Moutinho C, Pacheco J. Modal identification of concrete dams under natural excitation. J Civ Struct Health Monit 2021;11:465–84. http://dx.doi.org/10.1007/s13349-020-00462-9.
[34] Santamarta-Cerezal JC, González-Gonzálves JJ. Technical development and characteristics of dam engineering in the canary islands. Rev Obras Públ 2012;(3530):33–50.
[35] Documento XYZT. Presa de soria. Tech. rep., Dirección General de Obras Hidráulicas. Ministerio de Obras Públicas y Transportes; 1991.
[36] Infraestructura de datos espaciales de canarias. Modelo de terreno LIDAR. 2017, http://www.idecanarias.es.
[37] Domínguez J. Boundary elements in dynamics. 7th ed.. Computational Mechanics Publications & Elsevier Applied Science; 1993.
[38] Achenbach JD. Wave propagation in elastic solids. North Holland; 1973.
[39] Andersen L. Linear elastodynamic analysis. Department of Civil Engineering, Aalborg University; 2006.
[40] Maeso O. Modelo para el análisis sísmico de presas bóveda incluyendo los efectos de interacción suelo–agua–estructura (Ph.D. thesis), Universidad de Las Palmas de Gran Canaria; 1992, https://accedacris.ulpgc.es/handle/10553/1852.
[41] Aznárez JJ. Efecto de los fenómenos de interacción incluyendo factores espaciales y sedimentos de fondo en la respuesta sísmica de presas bóveda (Ph.D. thesis), Universidad de Las Palmas de Gran Canaria; 2002, https://accedacris.ulpgc.es/handle/10553/19508.
[42] Hall JF, Chopra AK. Dynamic analysis of arch dams including hydrodynamic effects. ASCE J Eng Mech 1983;109(1):149–67.
[43] Shul'man SG. Seismic pressure of water on hydraulic structures. CRC Press; 1987.

[44] Weber B. Rational transmitting boundaries for time-domain analysis of dam-reservoir interaction. Institut für baustatik und konstruktion. Eidgenössische technische hochschule Zurich, Basel: Birkhäuser; 1994.
[45] Eringen AC, Suhubi ES. Elastodynamics, Vol II. Linear theory. Academic Press; 1975.
[46] Reynders E, Magalhães F, De-Roeck G, Cunha A. Merging strategies for multi–setup operational modal analysis: application to the Luiz I steel arch bridge. In: Proceedings of the 26th international modal analysis conference, Vol. 36; 2009, p. 115–27.
[47] Amador SDR, Brincker R. Robust multi–dataset identification with frequency domain decomposition. J Sound Vib 2021;116207.
[48] Bendat JS, Piersol AG. Engineering applications of correlation and spectral analysis. New York: John Wiley & Sons; 1980.
[49] Conde López ER, Toledo Municio MA, Salete Casino E. Optimization of numerical models through instrumentation data integration: Digital twin models for dams. Comput Math Methods 2021;3(6). http://dx.doi.org/10.1002/cmm4.1205.
[50] Zhu X, Bao T, Yeoh JKW, Jia N, Li H. Enhancing dam safety evaluation using dam digital twins. Struct Infrastruct Eng 2021. http://dx.doi.org/10.1080/15732479.2021.1991387.